Magnon topology and thermal Hall effect in trimerized triangular lattice antiferromagnet

Kyung-Su Kim,[1,2] Ki Hoon Lee ●,[1,2,*] Suk Bum Chung,[3,4,5] and Je-Geun Park[1,2]

[1]*Department of Physics and Astronomy, Seoul National University, Seoul 08826, Republic of Korea*
[2]*Center for Correlated Electron Systems, Institute for Basic Science (IBS), Seoul 08826, Republic of Korea*
[3]*Department of Physics, University of Seoul, Seoul 02504, Republic of Korea*
[4]*Natural Science Research Institute, University of Seoul, Seoul 02504, Republic of Korea*
[5]*School of Physics, Korea Institute for Advanced Study, Seoul 02455, Korea*

The nontrivial magnon band topology and its consequent responses have been extensively studied in two-dimensional magnetisms. However, the triangular lattice antiferromagnet (TLAF), the best-known frustrated two-dimensional magnet, has received less attention than the closely related Kagome system, because of the spin-chirality cancellation in the umbrella ground state of the undistorted TLAF. In this paper, we study the band topology and the thermal Hall effect (THE) of the TLAF with (anti-)trimerization distortion under the external perpendicular magnetic field using the linearized spin wave theory. We show that the spin-chirality cancellation is removed in such case, giving rise to the nontrivial magnon band topology and the finite THE. Moreover, the magnon bands exhibit band topology transitions tuned by the magnetic field. We demonstrate that such transitions are accompanied by the logarithmic divergence of the first derivative of the thermal Hall conductivity. Finally, we examine the above consequences by calculating the THE in the hexagonal manganite YMnO₃, well known to have antitrimerization.

I. INTRODUCTION

The band topology has been extensively studied in the last decade for various quasiparticle excitations [1–10], including magnon, the elementary excitation of a magnetically ordered system. As the magnetic ordering breaks the time-reversal symmetry (TRS), it is natural to expect the magnon band structures analogous to that of the Weyl semimetal and the anomalous quantum Hall insulator [11–20]. In collinear phases, many magnon models with topological band structures were proposed [21–26]; however, there are only a few studies in noncollinear magnetic phases [15,18,27–29].

The band topology is closely related to transverse transport, and the thermal Hall effect (THE) is the most distinctive response expected from a TRS broken phase like magnetism. But the TRS breaking is only a necessary condition for having a finite THE, and whether a system shows a finite THE or not is also determined by its crystal symmetry. For example, in the collinear antiferromagnetic honeycomb lattice, while the spin Nernst effect can be nonzero, the THE is forbidden by the symmetry constraint that forces a zero Chern number [21–23]. More generally, a coplanar magnetic system without the spin-orbit coupling (SOC) cannot host a finite THE due to the effective TRS, which is the combination of the ordinary time-reversal and the π spin rotation around the axis normal to the spin plane [30]. Hence, in the absence of SOC, a noncoplanar spin configuration is necessary for the finite THE.

The simplest and yet most studied two-dimensional model hosting a noncoplanar phase is a triangular lattice antiferromagnet (TLAF) under a perpendicular external magnetic field. However, to our best knowledge, in spite of the noncoplanar spin ordering, little is known of the magnon band topology and transverse response of TLAF. This is due to the chirality cancellation in an undistorted TLAF, prohibiting a finite THE. This situation is very different from a Kagome lattice, another archetypical frustrated lattice, which has been widely studied in various contexts of band topology [17–19,27,28].

In this paper, we study the magnon band topology and the THE of the (anti)trimerized TLAF under the perpendicular magnetic field using the linearized spin wave theory. We clarify that the effective PT symmetry forces THE to vanish for the undistorted TLAF even under the perpendicular magnetic field. However, the (anti)trimerization distortion removes this symmetry, allowing a finite THE. Our study shows how the band topology of the TLAF depends on the distortion strength and the magnetic field, with the gap closings at the band topology transitions. Remarkably, these transitions are characterized by a logarithmic divergence in the first derivative of the thermal Hall conductivity. Such singularity behavior may be experimentally observed at zero magnetic field, where we found the strongest divergence due both to a quadratic band crossing at Γ and multiple linear band crossings. Finally, as a real experimental system, we estimate the size of magnon THE in YMnO₃, the material in which the antitrimerization is already observed [31].

II. MODEL

In this paper, we study the following anisotropic spin model on a triangular lattice with a magnetic field along the z
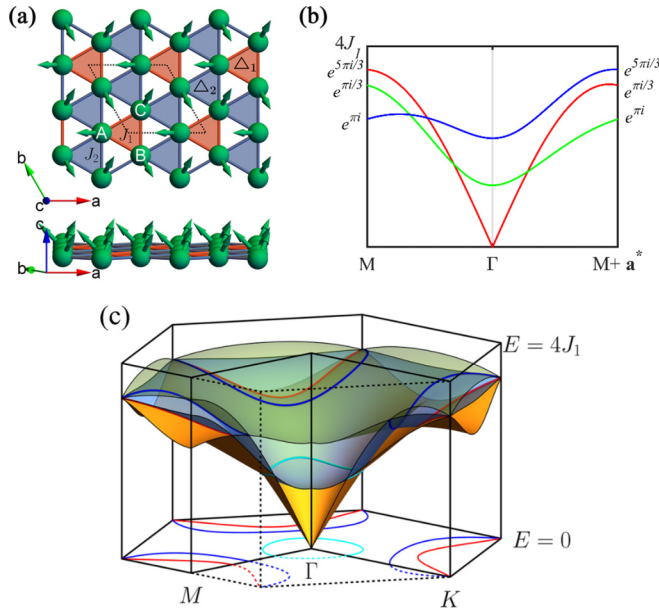
---

*kihoonlee@snu.ac.kr

FIG. 1. (a) The umbrella phase of TLAF. Red and blue equilateral triangles have different Heisenberg exchange coupling constants J_1 and J_2, respectively. (b) The magnon band structure of the $J_1 = J_2 = 1$ case with $h = 1$ and $D^z = 0.3$ along M to $M + \mathbf{a}^*$. Each band is classified according to the eigenvalues $\lambda e^{-i\mathbf{k}\cdot\mathbf{t}}$ of $\{g|\mathbf{t}\}$: $\lambda = 1$ (red), $e^{2\pi i/3}$ (green), and $e^{-2\pi i/3}$ (blue). Numbers on the left and right are $\lambda e^{-i\mathbf{k}\cdot\mathbf{t}}$ evaluated at the corresponding momentum. (c) The magnon band structure in the whole momentum space. The lines on the $E = 0$ plane is the projection of nodal lines.

axis:

$$\mathcal{H} = J_1 \sum_{\text{intra}} \mathbf{S}_i \cdot \mathbf{S}_j + J_2 \sum_{\text{inter}} \mathbf{S}_i \cdot \mathbf{S}_j + D^z \sum_i \left(\mathrm{S}_i^z\right)^2 \\ - h \sum_i \mathrm{S}_i^z, \tag{1}$$

where $J_1 > 0, J_2 > 0$ and $D^z > 0$. Here J_1 and J_2 denote intra- and intertrimer exchange constants as shown in Fig. 1(a), and $h = g\mu_B B$, where $g \approx 2$ is the g-factor and μ_B is the Bohr magneton.

First, we discuss the ground state of our model Eq. (1), where we assume classical spins ($S \to \infty$). The undistorted triangular lattice (i.e., $J_1 = J_2$) has been studied extensively [32–34]. In such a case, for $D^z = 0$, we have a three-sublattice ground-state structure subject to the constraint $\mathbf{S}_A + \mathbf{S}_B + \mathbf{S}_C = \mathbf{M}_\triangle = \hat{\mathbf{z}}h/3J$, where A, B, and C are the indices of the spins making a triangle as depicted in Fig. 1(a) and $\mathbf{M}_\triangle$ is the sum of the spins. This constraint fixes only three out of six free parameters (two for each spin sublattice) so the classical ground state manifold is highly degenerate. Adding a two-ion anisotropy in a XXZ model lifts this classical accidental degeneracy, selecting an umbrella structure as the unique ground state [33]. We instead introduced the single-ion easy-plane anisotropy, which plays a similar role as the two-ion anisotropy. As in the XXZ model, the single-ion easy-plane anisotropy in Eq. (1) would select the umbrella configuration which has the smallest z component of the spins among the classical ground state manifold, which includes V, Y, and

umbrella phase [33]. A similar argument can be made for the case $J_1 \neq J_2$ by rearranging the Hamiltonian of Eq. (1) as

$$\mathcal{H} = J_1 \sum_{\triangle \in \triangle_1} \left[\mathbf{M}_\triangle - \hat{\mathbf{z}}\frac{h}{3J_{\text{eff}}}\right]^2 + J_2 \sum_{\triangle \in \triangle_2} \left[\mathbf{M}_\triangle - \hat{\mathbf{z}}\frac{h}{3J_{\text{eff}}}\right]^2 \\ + D^z \sum_i \left(\mathrm{S}_i^z\right)^2 + (\text{const}), \tag{2}$$

where $3J_{\text{eff}} = J_1 + 2J_2$, and $\triangle_1$ and $\triangle_2$ are both the sets of equilateral triangles but with different side lengths as in Fig. 1(a). It can be also readily shown that in the absence of an easy-plane anisotropy we have the same three-sublattice structure subject to the constraint

$$\mathbf{S}_A + \mathbf{S}_B + \mathbf{S}_C = \hat{\mathbf{z}}\frac{h}{3J_{\text{eff}}}. \tag{3}$$

Now the easy-plane anisotropy selects the umbrella ground state as in the $J_1 = J_2$ case. And by a suitable parametrization of the spins in sublattices, i.e., $\mathbf{S}_\alpha = (\sin\theta\cos\phi_\alpha, \sin\theta\sin\phi_\alpha, \cos\theta)$ with ϕ_α's making $120°$ to each other, we find the tilting angle $\theta = \cos^{-1}(h/h_c)$, where $h_c = (9J_{\text{eff}} + 2D^z)S$. Hence, our model Eq. (1) has a simple ground-state phase diagram with the umbrella structure below the saturation field h_c and the fully polarized phase above. We note that even though the quantum fluctuation favors competing coplanar phases over the umbrella phase, a sufficiently large easy-plane anisotropy and/or an antiferromagnetic interlayer coupling stabilizes the umbrella phase [35].

III. SPIN WAVE ANALYSIS

We perform the Holstein-Primakoff (HP) transformation on Eq. (1) with the umbrella structure ground state: $\mathrm{S}^n = S - a^\dagger a$, $\mathrm{S}^+ \simeq \sqrt{2S}a$ and $\mathrm{S}^- \simeq \sqrt{2S}a^\dagger$, where n is the local magnetization direction,

$$\mathcal{H} = \frac{1}{2}\sum_{\alpha\beta\mathbf{k}} \psi_{\alpha\mathbf{k}}^\dagger H_{\alpha\beta}(\mathbf{k})\psi_{\beta\mathbf{k}}, \tag{4}$$

where $\psi_{\alpha\mathbf{k}}^\dagger = [a_{\alpha,\mathbf{k}}^\dagger, a_{\alpha,-\mathbf{k}}]$ and $a_{\alpha,\mathbf{k}}$ is the HP boson operator of sublattice $\alpha = A$, B, C, and momentum $\mathbf{k}$. The diagonalized form of the Hamiltonian is $\mathcal{H} = \frac{1}{2}\sum_{\eta,\mathbf{k}} (E_{\mathbf{k}}\gamma_{\eta\mathbf{k}}^\dagger\gamma_{\eta\mathbf{k}} + E_{\eta,-\mathbf{k}}\gamma_{\eta,-\mathbf{k}}\gamma_{\eta,-\mathbf{k}}^\dagger)$, where $\sum_\eta [\gamma_{\eta,\mathbf{k}}^\dagger, \gamma_{\eta,-\mathbf{k}}] T_{\eta\alpha\mathbf{k}}^\dagger = \psi_{\alpha\mathbf{k}}^\dagger$ and $T_{\mathbf{k}}$ is the paraunitary matrix (i.e., $T_{\mathbf{k}}^\dagger\sigma_3 T_{\mathbf{k}} = T_{\mathbf{k}}\sigma_3 T_{\mathbf{k}}^\dagger = \sigma_3$) diagonalizing $H(\mathbf{k})$ [36]. The Berry curvature is then defined as $\Omega_n^z(\mathbf{k}) = i\epsilon_{\mu\nu z}[\sigma_3\partial_{k_\mu}T_{\mathbf{k}}^\dagger\sigma_3\partial_{k_\nu}T_{\mathbf{k}}]_{nn}$. There are three magnon bands from three sublattices with a gapless linear Goldstone boson near Γ from the breaking of U(1) spin-rotation symmetry around the z axis [37].

Now in the undistorted case ($J_1 = J_2$), a "nonsymmorphic" spin space group symmetry protects nodal lines and triple degenerate points at K points [38,39] [Figs. 1(b)–1(c)]. To understand this, observe first that since the spin orderings of three sublattices in the umbrella state are related by the $120°$ spin rotation around the z axis, $\{g|\mathbf{t}\} = \{\exp(2\pi i S^z/3)\}|(2\mathbf{a} + \mathbf{b})/3\}$ is the symmetry of the system, where $\mathbf{a}$ and $\mathbf{b}$ are the primitive lattice vectors [Fig. 1(a)]. Here g leaves $\mathbf{k}$ invariant, and thus we can choose the

Bloch states to be eigenstates of $\{g|\mathbf{t}\}$: $\{g|\mathbf{t}\}|u_{\mathbf{k}}^{\lambda}\rangle = \lambda e^{-i\mathbf{k}\cdot\mathbf{t}}|u_{\mathbf{k}}^{\lambda}\rangle$, where $\lambda = 1$, $e^{\pm 2\pi i/3}$ since $\{g|\mathbf{t}\}^3|u_{\mathbf{k}}^{\lambda}\rangle = \{\hat{1}|2\mathbf{a}+\mathbf{b}\}|u_{\mathbf{k}}^{\lambda}\rangle = e^{-3i\mathbf{k}\cdot\mathbf{t}}|u_{\mathbf{k}}^{\lambda}\rangle$. Now, for $\mathbf{k} \to \mathbf{k}+\mathbf{a}^*$ ($\mathbf{k}+\mathbf{b}^*$), where $\mathbf{a}^*$ and $\mathbf{b}^*$ are the reciprocal primitive vectors corresponding to $\mathbf{a}$ and $\mathbf{b}$, we have $\lambda \to \lambda e^{2\pi i/3}$ ($\lambda e^{-2\pi i/3}$), alternating among the three eigenstates [Fig. 1(b)]. Thus, in general the three magnon branches meet an even number of times (at least twice) as they cross BZ. In Fig. 1(b), we show the case for $M \to M+\mathbf{a}^*$ where there are four such crossings. This story holds for any $\mathbf{k} \to \mathbf{k}+\mathbf{a}^*$, leading to the nodal line structures as shown in Fig. 1(c). In addition, at two K points we have additional C_{3z} symmetry, relating three eigenstates: $\{g|\mathbf{t}\}C_{3z}|u_{\mathbf{k}}^{\lambda}\rangle = C_{3z}\{g|C_{3z}^{-1}\mathbf{t}\}|u_{\mathbf{k}}^{\lambda}\rangle = \lambda e^{\pm 2\pi i/3}e^{-i\mathbf{k}\cdot\mathbf{t}}C_{3z}|u_{\mathbf{k}}^{\lambda}\rangle$. Therefore, $\{g|\mathbf{t}\}$ and C_{3z} protect the threefold degeneracy at two K points.

All the nodal lines and triple degenerate points are gapped in the presence of the trimerization distortion in Eq. (1), as the spin nonsymmorphic symmetry is no longer present, generating the Berry curvature $\Omega_n^z(\mathbf{k})$ near these gaps. Since the three bands are now gapped, the Chern number for individual band can be defined.

IV. BAND TOPOLOGY AND THERMAL HALL EFFECT

In Fig. 2, we show Chern numbers $C_n = \frac{1}{2\pi}\int_{BZ}\Omega_n^z(\mathbf{k})d^2k$ for each band with the band topology transition lines and the intrinsic thermal Hall conductivity in the $h-J_2/J_1$ space for several values of D^z. Here we used the parametrization
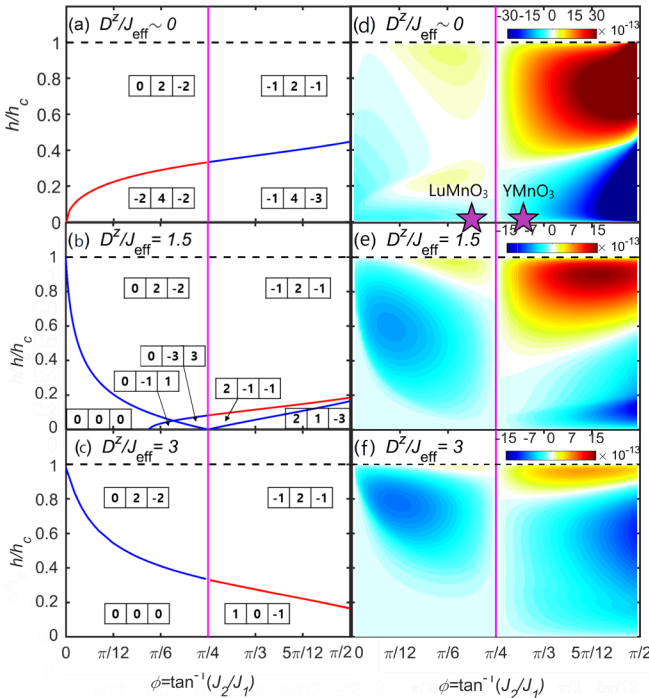

FIG. 2. (a)–(c) The band topology diagram for three different values of single-ion easy-plane anisotropy, where three Chern numbers, from the top band to the bottom bands, are denoted in the box. For (a) and (d), we assumed a small but finite easy-plane anisotropy in order to stabilize the umbrella ground state. (d)–(f) show the thermal Hall conductivity at $T = J_{\mathrm{eff}}/k_B$. In (d) we display the expected trimerization magnitude $J_2/J_1 \sim 1.2$ and $J_2/J_1 \sim 0.8$ for YMnO$_3$ and LuMnO$_3$, respectively.

$J_1 = \cos\phi$ and $J_2 = \sin\phi$. The thermal Hall conductivity at temperature $T = J_{\mathrm{eff}}/k_B$ is calculated using the following formula [40,41]:

$$\kappa_{xy} = \frac{k_B^2 T}{(2\pi)^2\hbar}\sum_n\int_{BZ}c_2(\rho_{n,\mathbf{k}})\Omega_n^z(\mathbf{k})d^2k, \qquad (5)$$

where $\Omega_n^z(\mathbf{k})$ is the Berry curvature of the nth band at momentum $\mathbf{k}$. Here, the c_2 function is given by $c_2(\rho) = (1+\rho)(\log\frac{1+\rho}{\rho})^2 - (\log\rho)^2 - 2\mathrm{Li}_2(-\rho)$ with $\mathrm{Li}_2(z)$ the polylogarithm function and $\rho_{n,\mathbf{k}} = 1/(\exp(\epsilon_{n,\mathbf{k}}/k_B T)-1)$, where $\epsilon_{n,\mathbf{k}}$ is the energy of the nth band at momentum $\mathbf{k}$ and ρ is the Bose distribution function. T, $\epsilon_n(\mathbf{k})$ and thus κ_{xy} are normalized in units of $S\sqrt{J_1^2+J_2^2}$.

Let us make a general remark on the condition for a finite Chern number and THE in magnetic systems. First, note that even though the TRS is broken, the magnetic systems with the coplanar spin ordering possess effective TRS in the absence of SOC, forbidding finite Hall responses [30]. More explicitly, the time reversal followed by $180°$ spin rotation around the axis normal to the plane, $\tilde{T} = \exp(-i\pi S^z)T$, is the symmetry of the system in such a case. This symmetry imposes a constraint on the Berry curvature, $\Omega_n^z(\mathbf{k}) = -\Omega_n^z(-\mathbf{k})$, enforcing both the band Chern number and the thermal Hall conductivity to be zero. However, if the system possesses a noncoplanar spin configuration with nonzero chirality $\chi = \mathbf{S}_A \cdot \mathbf{S}_B \times \mathbf{S}_C$, then the effective TRS is broken and we can expect a finite band Chern number and THE.

However, following the line (magenta) for an undistorted triangular lattice ($J_1 = J_2$) in Fig. 2, THE is zero even when a finite magnetic field is applied. It is because of the effective PT symmetry $\tilde{I} = \exp(-i\pi S^y)PT$, where the inversion center is at the middle of B and C in Fig. 1(a). In this case, we have $\Omega_n^z(\mathbf{k}) = -\Omega_n^z(\mathbf{k}) = 0$, also forbidding a finite Chern number and THE. This situation can also be understood heuristically in terms of spin chirality χ: Because χ has the opposite sign for the neighboring triangles, it cancels out and magnon feels no gauge field. Note that the constraint from the effective PT symmetry applies to the charge Hall effect in itinerant magnetic systems as well. In the presence of the (anti)trimerization ($J_1 \neq J_2$), the effective PT symmetry is absent. Now since there is no symmetry to enforce the Berry curvature to vanish, we expect a finite magnon THE.

We find that the magnon band structure exhibits a rich band topology diagram in the $h-J_2/J_1$ space. Since the three bands are separated from one another away from the $J_1 = J_2$ lines (magenta) and below the saturation field (dashed line) in the parameter space, the Chern numbers are well defined for the top, middle, and bottom bands, as denoted in Figs. 2(a)–2(c). On the red lines, there is an accidental gap closing between the top and middle bands, while on the blue lines, between the middle and bottom bands. We further find that all the degeneracies occur either at K points or on the Γ-M segment. Two accidental gap closings appear at the K point as the two K points are related by $M_{\mathbf{y}}T$, where $M_{\mathbf{y}}$ is the mirror operation about $y = 0$ plane, while three accidental gap closings appear for the Γ-M case as three Γ-M lines are related by C_{3z}. Hence, the topological band transition with the gap closings at K changes the Chern number by 2 and the one with the gap closings at Γ-M changes it by 3.

In Figs. 2(d)–2(f) we show the intrinsic contribution to the magnon thermal Hall conductivity. It has intriguing behavior, yet at first sight reveals no apparent relation to the band topology diagram of Figs. 2(a)–2(c). Interestingly, there was a numerical observation of the singular behavior of κ_{xy} at the phonon band topology transition point [42]; however, the appropriate explanation was not provided. Here, we found that the band topology transition of a free bosonic system manifests itself as the logarithmic divergence in the first derivative of κ_{xy} at the transition point both for the linear and higher-order band crossing. To see it clearly, let us assume without loss of generality that the transition occurs at $p = 0$, where p could be any parameter inducing a band topology transition (e.g., external magnetic field) with gap closing between two bands at $\mathbf{k} = 0$ and $E = \mathcal{E}_0$, leading to a Weyl point in the $\tilde{\mathbf{k}} = (k_x, k_y, p)$ space. In the case of the isotropic single Weyl point, i.e., $H(\tilde{\mathbf{k}}) = \mathcal{E}_0 - \tilde{\mathbf{k}} \cdot \sigma$, the singular contribution of the THE is $\tilde{\Omega}_{n,\mathbf{k}}^p c_2(\rho_{n,\mathbf{k}}) = \pm \frac{p}{2(k^2+p^2)^{3/2}} c_2[\rho(\mathcal{E}_0 \pm \epsilon_{\mathbf{k}}^p)]$ for the upper and lower bands, respectively, where $\epsilon_{\mathbf{k}}^p = \sqrt{k^2 + p^2}$. Now, since $c_2[\rho(\mathcal{E}_0 + \epsilon_{\mathbf{k}}^p)] - c_2(\rho(\mathcal{E}_0 - \epsilon_{\mathbf{k}}^p)) \propto \epsilon_{\mathbf{k}}^p$ for small k and p, one immediately notices the logarithmic divergence of the first derivative of $\tilde{\kappa}_{xy}$ at the transition point $p = 0$:

$$\frac{\partial}{\partial p} \tilde{\kappa}_{xy}^p \propto \frac{\partial}{\partial p} \int_{k<k_c} d^2k\, \Omega_{n,\mathbf{k}} \epsilon_{\mathbf{k}}^p \propto \log|p| + \cdots . \quad (6)$$
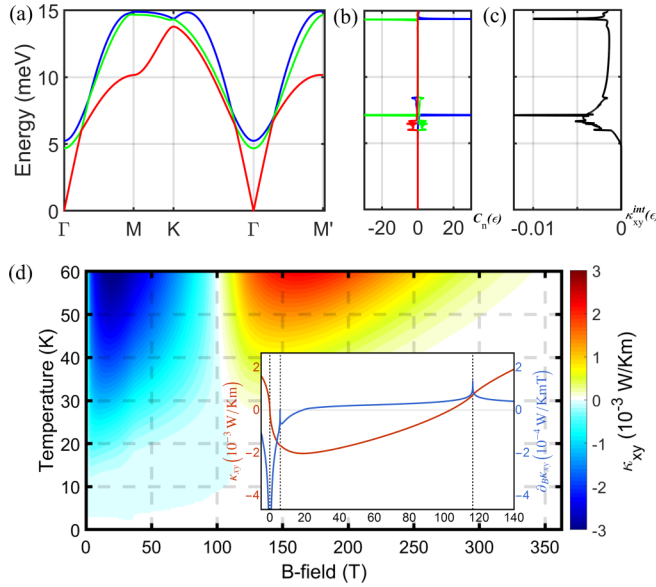

FIG. 3. (a) Magnon band structure of YMnO$_3$ with $B = 5$ T. (b) Energy-resolved Chern number. (c) Integrated thermal Hall conductivity $\kappa_{xy}^{\text{int}}(\epsilon)$ as defined in the text at $T = 40$ K. The thermal Hall conductivity is $\kappa_{xy} = -1.53 \times 10^{-3}$ W/Km. (d) Temperature and magnetic-field dependence of calculated thermal Hall conductivity of YMnO$_3$. The inset is κ_{xy} and $\partial_B \kappa_{xy}$ at 40 K, where the singularities appear at the band topology transition points (dotted lines): $B = 0$, 5.9, and 116.3 T. The band Chern numbers, from the top to the bottom band, are $[-2, -1, 3]$ ($B < 0$ T), $[2, 1, -3]$ (0 T $< B < 5.9$ T), $[-1, 4, -3]$ (5.9 T $< B < 116.3$ T), and $[-1, 2, -1]$ (116.3 T $< B < 363$ T), respectively. At $B = 0$, κ_{xy} and the band Chern numbers reverse their sign, because $B < 0$ and $B > 0$ sectors are related by C_{2x}.

This result can be easily generalized to include multiple gap closings and the anisotropy. In the case of the multi-Weyl point, $H(\tilde{\mathbf{k}}) = \mathcal{E}_0 - (k^n \cos(n\phi), k^n \sin(n\phi), p) \cdot \sigma$, where $\tan\phi = k_y/k_x$, we have $\tilde{\Omega}_{n,\mathbf{k}}^p \epsilon_{\mathbf{k}}^p = \frac{pn^2 k^{2(n-1)}}{k^{2n}+p^2}$, leading to the same logarithmic singularity but with a higher-order band crossing at the transition point. We note that our model exhibits both accidental linear band crossings and essential quadratic band crossings; the latter occurs at Γ when $h = 0$ due to the combination of C_3 point symmetry group and $\tilde{T}$ [37]. We corroborate the above results by the numerical calculation of the THE for YMnO$_3$ [the inset of Fig. 3(d)], which we will discuss below in more detail.

V. THERMAL HALL EFFECT IN YMnO$_3$

As a real experimental example, we consider YMnO$_3$, in which Mn^{3+} ions with $S = 2$ form a quasi-2D TLAF with the interlayer distance of $c/2 = 5.7$ Å. The strong spin-lattice coupling was previously reported in this multiferroic material, where the antitrimerization distortion of the lattice occurs at $T_N = 75$ K [31]. The magnetic structure and the origin of multiferroicity of the compound have long been the subject of debate. In particular, the lattice distortion was at first thought to lead to a large modulation in the exchange constant J [43,44], but a more recent study shows a smaller (yet still significant) effect with $J_2/J_1 \sim 1.2$ [45,46]. Here, we assume the realistic parameters for the magnetic Hamiltonian of YMnO$_3$ and calculate the THE: $J_1 = 2$ meV, $J_2 = 2.4$ meV, and $D^z = 0.3$ meV.

First, we show the magnon band structure along with energy-resolved Chern number $C_n(\epsilon) = \frac{1}{2\pi} \int_{\text{BZ}} \delta(\epsilon_{n,\mathbf{k}} - \epsilon) \Omega_n^z(\mathbf{k}) d^2k$ and the integrated thermal Hall conductivity $\kappa_{xy}^{\text{int}}(\epsilon) = \frac{k_B^2 T}{(2\pi)^2 \hbar} \sum_n \int_{\epsilon_{n,\mathbf{k}} < \epsilon} c_2(\rho_{n,\mathbf{k}}) \Omega_n^z(\mathbf{k}) d^2k$ for $B = h/g\mu_B = 5$ T and $T = 40$ K [Figs. 3(a)–3(c)]. Since $J_2/J_1 = 1.2$, which is not very far away from nodal semimetallike band structure ($J_1 = J_2$), we can see that band gaps are quite small and the Berry curvature is concentrated around these gaps. We next show the magnetic field and temperature dependence of κ_{xy}, plotted up to the saturation field $B_c \simeq 363$ T and $T = 60$ K $< T_N$ [Fig. 3(d)]. We observe that the THE is still large ($\kappa_{xy} \sim -10^{-3}$ W/Km) even for small magnetic fields (~ 10 T) at temperatures as low as 30 K. We emphasize that since the longitudinal thermal conductivity is measured to be $\kappa_{xx} \sim 10$ W/Km [47], the Hall angle $\kappa_{xy}/\kappa_{xx} \sim 10^{-4}$ of our result is in an observable range of experiments [48]. Furthermore, the THE shows the most profound signature of the singularity of κ_{xy}, as derived in Eq. (6), at zero magnetic field, where both the linear and quadratic crossings occur. Hence, we expect that the consequence of the band topology transition can be measured by a careful experiment in YMnO$_3$.

Before concluding, we remark that because of the large spin-lattice coupling in YMnO$_3$ [45], the phonon contribution to κ_{xy} may not be negligible [49]. In fact, even in the absence of trimerization, the effective PT symmetry, $\tilde{I} = \exp(-i\pi S^y)PT$, is still broken in the material when we consider nonmagnetic ions such as O^{2-}, and so magnetoelastic excitation may contribute appreciably to κ_{xy}. Therefore, the inclusion of phonon may change our calculation of the thermal

Hall conductivity, but the symmetry remains the same, so we should still expect the finite thermal Hall effect. We leave a detailed study on this issue as the focus of future study.

VI. CONCLUSION

In conclusion, we considered the trimerization distortion and the magnetic field on TLAF, which give rise to the nontrivial band topology and the finite THE. This leads to a variety of topologically distinct band structures, in contrast to a rather simple undistorted case [50,51]. As one crosses the band topology transition boundary, the first derivative of the thermal Hall conductivity shows a logarithmic divergence.

This establishes the clear relation between the bosonic band topology and the THE. We finally propose the hexagonal manganite family $RMnO_3$ with the $P6_3cm$ space group as the candidate material to detect such effects.

ACKNOWLEDGMENTS

[1] F. D. M. Haldane, Rev. Mod. Phys. **89**, 040502 (2017).

[2] M. Z. Hasan and C. L. Kane, Rev. Mod. Phys. **82**, 3045 (2010).

[3] X.-L. Qi and S.-C. Zhang, Rev. Mod. Phys. **83**, 1057 (2011).

[4] Y. Ando, J. Phys. Soc. Jpn. **82**, 102001 (2013).

[5] B. A. Bernevig and T. L. Hughes, *Topological Insulators and Topological Superconductors* (Princeton University Press, Princeton, 2013).

[6] C.-K. Chiu, J. C. Y. Teo, A. P. Schnyder, and S. Ryu, Rev. Mod. Phys. **88**, 035005 (2016).

[7] F. D. M. Haldane and S. Raghu, Phys. Rev. Lett. **100**, 013904 (2008).

[8] Z. Wang, Y. D. Chong, J. D. Joannopoulos, and M. Soljačić, Phys. Rev. Lett. **100**, 013905 (2008).

[9] P. A. McClarty, F. Krüger, T. Guidi, S. Parker, K. Refson, A. Parker, D. Prabhakaran, and R. Coldea, Nat. Phys. **13**, 736 (2017).

[10] R. Süsstrunk and S. D. Huber, Science **349**, 47 (2015).

[11] F.-Y. Li, Y.-D. Li, Y. B. Kim, L. Balents, Y. Yu, and G. Chen, Nat. Commun. **7**, 12691 (2016).

[12] K. Hwang, N. Trivedi, and M. Randeria, arXiv:1712.08170.

[13] S.-K. Jian and W. Nie, Phys. Rev. B **97**, 115162 (2018).

[14] Y. Su and X. R. Wang, Phys. Rev. B **96**, 104437 (2017).

[15] S. A. Owerre, J. Phys.: Condens. Matter **29**, 03LT01 (2017).

[16] S. A. Owerre, J. Phys.: Condens. Matter **29**, 185801 (2017).

[17] R. Chisnell, J. S. Helton, D. E. Freedman, D. K. Singh, R. I. Bewley, D. G. Nocera, and Y. S. Lee, Phys. Rev. Lett. **115**, 147201 (2015).

[18] P. Laurell and G. A. Fiete, Phys. Rev. B **98**, 094419 (2018).

[19] A. Mook, J. Henk, and I. Mertig, Phys. Rev. B **89**, 134409 (2014).

[20] L. Zhang, J. Ren, J.-S. Wang, and B. Li, Phys. Rev. B **87**, 144101 (2013).

[21] V. A. Zyuzin and A. A. Kovalev, Phys. Rev. Lett. **117**, 217203 (2016).

[22] R. Cheng, S. Okamoto, and D. Xiao, Phys. Rev. Lett. **117**, 217202 (2016).

[23] K. H. Lee, S. B. Chung, K. Park, and J.-G. Park, Phys. Rev. B **97**, 180401(R) (2018).

[24] S. K. Kim, H. Ochoa, R. Zarzuela, and Y. Tserkovnyak, Phys. Rev. Lett. **117**, 227201 (2016).

[25] X. S. Wang, Y. Su, and X. R. Wang, Phys. Rev. B **95**, 014435 (2017).

[26] K. Nakata, S. K. Kim, J. Klinovaja, and D. Loss, Phys. Rev. B **96**, 224414 (2017).

[27] S. A. Owerre, Phys. Rev. B **97**, 094412 (2018).

[28] S. A. Owerre, Phys. Rev. B **95**, 014422 (2017).

[29] N. Okuma, Phys. Rev. Lett. **119**, 107205 (2017).

[30] M.-T. Suzuki, T. Koretsune, M. Ochi, and R. Arita, Phys. Rev. B **95**, 094406 (2017).

[31] S. Lee, A. Pirogov, M. Kang, K. Jang, M. Yonemura, T. Kmiyama, S. Cheong, F. Gozzo, N. Shin, H. Kimura, Y. Noda, and J. Park, Nature **451**, 805 (2008).

[32] C. Griset, S. Head, J. Alicea, and O. A. Starykh, Phys. Rev. B **84**, 245108 (2011).

[33] D. Yamamoto, G. Marmorini, and I. Danshita, Phys. Rev. Lett. **112**, 127203 (2014).

[34] D. Sellmann, X.-F. Zhang, and S. Eggert, Phys. Rev. B **91**, 081104(R) (2015).

[35] G. Marmorini, D. Yamamoto, and I. Danshita, Phys. Rev. B **93**, 224402 (2016).

[36] J. Colpa, Physica A **93**, 327 (1978).

[37] See Supplemental Material at http://link.aps.org/supplemental/10.1103/PhysRevB.100.064412, which includes Refs. [52,53], for the representation of the HP boson Hamiltonian, the symmetry analysis, the band structure and Berry curvature plots for some parameters and the numerical fitting of κ_{xy} near band topology transitions.

[38] S. M. Young and C. L. Kane, Phys. Rev. Lett. **115**, 126803 (2015).

[39] S. M. Young and B. J. Wieder, Phys. Rev. Lett. **118**, 186401 (2017).

[40] R. Matsumoto and S. Murakami, Phys. Rev. B **84**, 184406 (2011).

[41] R. Matsumoto and S. Murakami, Phys. Rev. Lett. **106**, 197202 (2011).

[42] L. Zhang, J. Ren, J.-S. Wang, and B. Li, Phys. Rev. Lett. **105**, 225901 (2010).

[43] J. Oh, M. D. Le, J. Jeong, J. H. Lee, H. Woo, W.-Y. Song, T. G. Perring, W. J. L. Buyers, S.-W. Cheong, and J.-G. Park, Phys. Rev. Lett. **111**, 257202 (2013).

[44] H. J. Lewtas, A. T. Boothroyd, M. Rotter, D. Prabhakaran, H. Müller, M. D. Le, B. Roessli, J. Gavilano, and P. Bourges, Phys. Rev. B **82**, 184420 (2010).

[45] J. Oh, M. Le, H. Nahm, H. Sim, J. Jeong, T. Perring, H. Woo, K. Nakajima, S. Ohira-Kawamura, Z. Yamani, Y. Yoshida, H. Eisaki, S. Cheong, A. Chernyshev, and J. Park, Nat. Commun. **7** 13146 (2016).

[46] J. Varignon, S. Petit, A. Gellé, and M. Lepetit, J. Phys.: Condens. Matter **25**, 496004 (2013).

[47] P. A. Sharma, J. S. Ahn, N. Hur, S. Park, S. B. Kim, S. Lee, J.-G. Park, S. Guha, and S. W. Cheong, Phys. Rev. Lett. **93**, 177202 (2004).

[48] T. Ideue, T. Kurumaji, S. Ishiwata, and Y. Tokura, Nat. Mater. **16**, 797 (2017).

[49] S. Park and B.-J. Yang, Phys. Rev. B **99**, 174435 (2019).

[50] H. Katsura, N. Nagaosa, and P. A. Lee, Phys. Rev. Lett. **104**, 066403 (2010).

[51] S. Owerre, J. Phys.: Condens. Matter **29**, 385801 (2017).

[52] C. Fang, M. J. Gilbert, X. Dai, and B. A. Bernevig, Phys. Rev. Lett. **108**, 266802 (2012).

[53] Q.-F. Liang, R. Yu, J. Zhou, and X. Hu, Phys. Rev. B **93**, 035135 (2016).